Atmos. Meas. Tech., 8, 987–997, 2015
www.atmos-meas-tech.net/8/987/2015/
doi:10.5194/amt-8-987-2015

Atmospheric Measurement Techniques
Open Access

Measurements of $CH_3O_2NO_2$ in the upper troposphere

B. A. Nault[1], C. Garland[2], S. E. Pusede[2,*], P. J. Wooldridge[2], K. Ullmann[3], S. R. Hall[3], and R. C. Cohen[1,2]

[1]Department of Earth and Planetary Science, University of California at Berkeley, Berkeley, CA, USA
[2]Department of Chemistry, University of California at Berkeley, Berkeley, CA, USA
[3]Atmospheric Chemistry Division, National Center for Atmospheric Research, Boulder, CO, USA
[*]now at: NASA Langley Research Center, Hampton, VA, USA

Correspondence to: R. C. Cohen (rccohen@berkeley.edu)

Received: 2 September 2014 – Published in Atmos. Meas. Tech. Discuss.: 17 September 2014
Revised: 12 January 2015 – Accepted: 4 February 2015 – Published: 27 February 2015

Abstract. Methyl peroxy nitrate ($CH_3O_2NO_2$) is a non-acyl peroxy nitrate that is important for photochemistry at low temperatures characteristic of the upper troposphere. We report the first measurements of $CH_3O_2NO_2$, which we achieved through a new aircraft inlet configuration, combined with thermal-dissociation laser-induced fluorescence (TD-LIF) detection of NO_2, and describe the accuracy, specificity, and interferences to $CH_3O_2NO_2$ measurements. $CH_3O_2NO_2$ is predicted to be a ubiquitous interference to upper-tropospheric NO_2 measurements. We describe an experimental strategy for obtaining NO_2 observations free of the $CH_3O_2NO_2$ interference. Using these new methods, we made observations during two recent aircraft campaigns: the Deep Convective Clouds and Chemistry (DC-3) and the Studies of Emissions and Atmospheric Composition, Clouds, and Climate Coupling by Regional Surveys (SEAC4RS) experiments. The $CH_3O_2NO_2$ measurements we report have a detection limit ($S/N = 2$) of 15 pptv at 1 min averaging on a background of 200 pptv NO_2 and an accuracy of ±40 %. Observations are used to constrain the interference of pernitric acid (HO_2NO_2) to the $CH_3O_2NO_2$ measurements, as HO_2NO_2 partially decomposes (∼ 11 %) along with $CH_3O_2NO_2$ in the heated $CH_3O_2NO_2$ channel used to detect $CH_3O_2NO_2$.

1 Introduction

Methyl peroxy nitrate ($CH_3O_2NO_2$) is predicted to be abundant at temperatures below 240 K (Fig. 1), where it serves as a temporary reservoir of NO_x ($NO_x = NO + NO_2$). $CH_3O_2NO_2$ can be transported on regional scales moving NO_x from source to receptor regions and thus affecting O_3, OH, and other chemistry of the upper troposphere. The emphasis on low temperatures results from non-acyl peroxy nitrates, such as $CH_3O_2NO_2$ and pernitric acid (HO_2NO_2), having lower thermal stability and shorter lifetimes than acyl peroxy nitrates, such as peroxy acetyl nitrate (PAN) and peroxy propionyl nitrate (PPN) (∼ 100 kJ mol^{-1} for non-acyl peroxy nitrates vs. ∼ 120 kJ mol^{-1} for acyl peroxy nitrates).

The low thermal stability of $CH_3O_2NO_2$ poses analytical challenges. At room temperature, $CH_3O_2NO_2$'s lifetime is shorter than 1 s (Fig. 1). If the air sample is brought into a warm aircraft prior to detection, this very short lifetime results in substantial decomposition for residence times longer than even 0.1 s (Fig. 2). As a result of the decomposition of $CH_3O_2NO_2$, there is also a positive interference to NO_2 measurements with residence times at warm temperatures longer than 0.1 s. For NO_2 measurements, the interference was quantified to be as much as 43 % during a study over Canada in springtime (Browne et al., 2011). Thus, in addition to interest in measurement of $CH_3O_2NO_2$, it is essential to understand $CH_3O_2NO_2$ to correct NO_2 measurements for its presence. Alternatively, in the absence of such a correction, it is necessary to interpret NO_2 measurements as XNO_2, where XNO_2 is the sum of ambient NO_2 and some or all of non-acyl peroxy nitrates (Browne et al., 2011).

There have been no prior direct measurements of ambient $CH_3O_2NO_2$. The only in situ information about $CH_3O_2NO_2$ stems from indirect measurements of the sum of $CH_3O_2NO_2$ and HO_2NO_2 by calculating the difference between total peroxy nitrate measurements and measurements of PAN and PPN (Murphy et al., 2004) and analysis of temperature-dependent deviations of NO_2 observations from photosta-

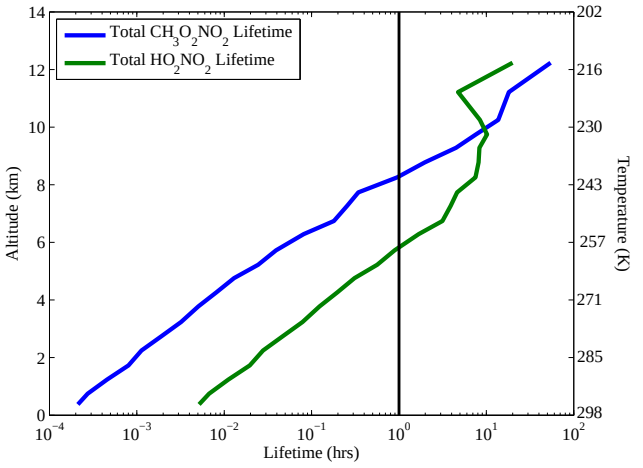

Figure 1. Calculated mean total lifetime profile of $CH_3O_2NO_2$ (blue) and HO_2NO_2 (green) for typical conditions observed during DC-3 in the daytime. The total lifetime is calculated using observed OH, photolysis rates, and temperatures along with the rate constants listed in Table 2 and measurements in Table 3. The black line marks the region where the non-acyl peroxy nitrates have a lifetime longer than 1 h.

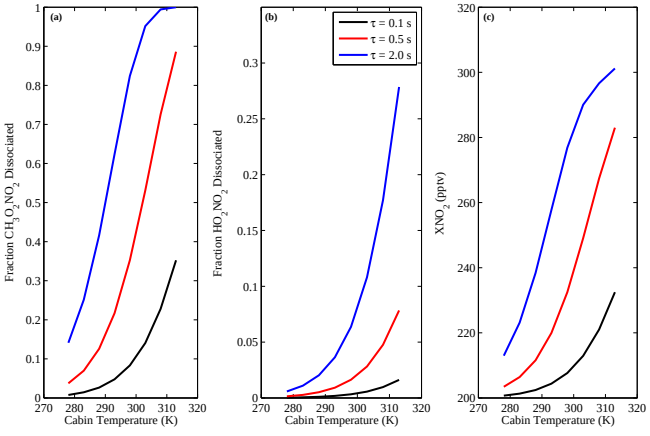

Figure 2. Calculated fraction of **(a)** $CH_3O_2NO_2$ and **(b)** HO_2NO_2 dissociated at residence times of 2.0 (blue), 0.5 (red) and 0.1 s (black), and cabin temperatures ranging from 275 to 310 K. The calculations are for ambient pressures of 230 hPa and ambient temperatures of ∼ 225 K. **(c)** XNO_2 ($XNO_2 = NO_2 +$ fraction dissociated $CH_3O_2NO_2$ and fraction dissociated HO_2NO_2) as a function of the residence times and cabin temperatures used in **(a)** and **(b)**. We use the median mixing ratios of NO_2 (200 pptv), $CH_3O_2NO_2$ (90 pptv), and HO_2NO_2 (40 pptv) observed between 220 and 230 K during DC-3.

tionary state (e.g., Browne et al., 2011). Murphy et al. (2004) showed that the sum of non-acyl peroxy nitrates contributes a large fraction of the NO_y budget (10–22 %) in aged air masses. However, the individual contributions from $CH_3O_2NO_2$ and HO_2NO_2 were only identified modeling the sum. Browne et al. (2011) calculated that $CH_3O_2NO_2$ mixing ratios of ∼ 25 pptv should be expected; however, their calculations along flight tracks were limited to air samples at photostationary steady state.

Using the limited observational inferences as a guide, Browne et al. (2011) added $CH_3O_2NO_2$ chemistry to a global chemical transport model (GEOS-Chem) and used the model to explore the role of $CH_3O_2NO_2$ in the upper troposphere (T ∼ 210–250 K), allowing study of conditions that do not reach steady state. They found that $CH_3O_2NO_2$ chemistry reduced NO_x mixing ratios with measurable effects on O_3, HNO_3, OH, and HO_2. They showed that $CH_3O_2NO_2$ mixing ratios peak in the summer due to more rapid photochemistry, and that biomass burning or deep convection can increase $CH_3O_2NO_2$ mixing ratios by a factor of ∼ 3 over mean atmospheric mixing ratios.

Following on these studies demonstrating that an understanding of $CH_3O_2NO_2$ is important, we developed new configurations of the UC Berkeley thermal-dissociation laser-induced fluorescence (TD-LIF) instrument inlet aimed at unambiguous measurements of NO_2 and $CH_3O_2NO_2$. In this paper, we describe the design and performance of a modified inlet for the TD-LIF instrument; provide recommendations for minimizing and eliminating $CH_3O_2NO_2$ interferences to NO_2; and present observations of $CH_3O_2NO_2$ from two recent aircraft campaigns: the Deep Convective Clouds and Chemistry (DC-3) and the Studies of Emissions and Atmospheric Composition, Clouds, and Climate Coupling by Regional Surveys (SEAC4RS) experiments. These measurements are the first in situ measurements providing specific information about atmospheric $CH_3O_2NO_2$.

2 Thermal-dissociation laser-induced fluorescence detection of $CH_3O_2NO_2$

2.1 Thermal-dissociation laser-induced fluorescence

The TD-LIF instrument has been described previously (Thornton et al., 2000; Day et al., 2002; Wooldridge et al., 2010). Briefly, NO_2 is measured by laser-induced fluorescence (Thornton et al., 2000) with supersonic expansion (Cleary et al., 2002). A 7 kHz, Q-switched, frequency-doubled Nd:Yag laser pumps a tunable dye laser producing ∼ 20 ns pulses at 585 nm and a bandwidth of 0.06 cm^{-1}. The dye laser is tuned on (9 s) and off (3 s) an isolated rovibronic feature of the jet-cooled NO_2 at 585 nm. The ratio between the peak and background NO_2 fluorescence is 10 : 1, sampling from an ambient pressure of 1 atm. The laser light is focused through two multipass White cells. Red-shifted fluorescence (wavelengths greater than 700 nm) of excited NO_2 is detected at a right angle to the excitation using a red-sensitive photomultiplier tube (Hamamatsu H7421-50). Scattered light is minimized using time-gated detection and dielectric band-pass filters that block light at wavelengths less than 700 nm. Fluorescence counts are collected at 4 Hz

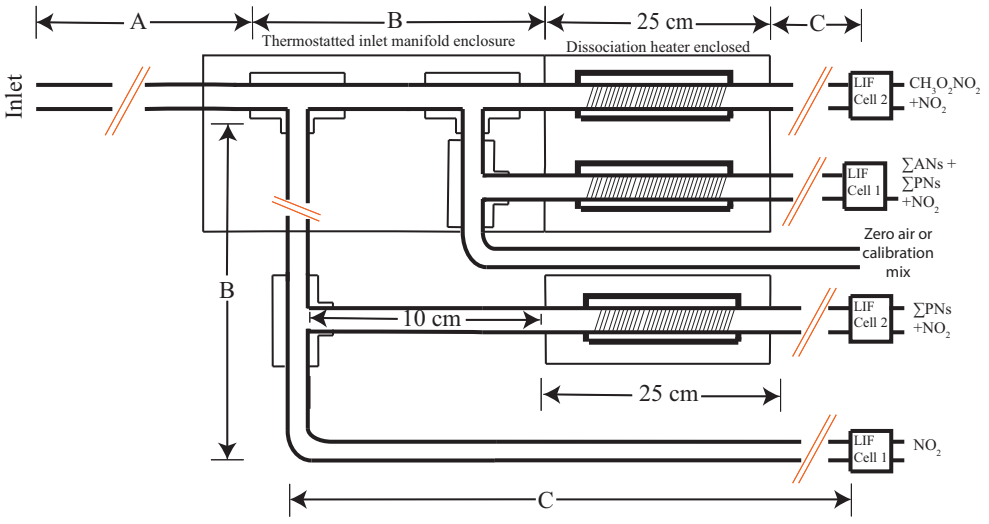

Figure 3. Schematic of the TD-LIF inlet sampling manifold. Arrows and letters refer to lengths referenced in Table 1. The species measured in each channel is shown at the right, where $\Sigma PNs \equiv PAN + PPN + CH_3O_2NO_2 + HO_2NO_2 + ...$ and $\Sigma ANs \equiv$ the sum of gas and aerosol alkyl and multifunctional nitrates.

and reported as 1 s averages. For these measurements, calibrations were performed at least every hour during a level flight leg or after a significant change in altitude using a 4.67 ($\pm$0.26) ppmv NO_2 standard (Praxair) diluted to $\sim$ 2–8 ppbv in zero air. The accuracy and stability of this reference gas was compared against a library of other NO_2 standards in our laboratory. Measurements of zero were obtained with similar frequency. Fluorescence quenching by water vapor is accounted for (Thornton et al., 2000) using diode laser hygrometer (DLH) measurements of H_2O (Diskin et al., 2002).

The TD-LIF instrument samples ambient air using a large flow carried through a 35 mm internal diameter (i.d.) tube from the undisturbed free stream either by ram pressure from a partially plugged shroud at the inlet tip (Arctic Research of the Composition of the Troposphere from Aircraft and Satellites, or ARCTAS; DC-3) or carried through a 16 mm i.d. tube by a 120L min^{-1} sample pump (SEAC4RS). The core of that flow was subsampled by a short ($\sim$ 0.10 m long) tube where air had a residence time of $\sim$ 0.03 s and then split into multiple sample lines for detection of specific categories of NO_y (Fig. 3). For $CH_3O_2NO_2$ detection, the sample is passed directly through a heated quartz tube (i.d. $\sim$ 4.3 mm, $T \approx 60$ °C) for 0.06–0.08 s followed by PFA tubing (i.d. $\sim$ 3.2 mm) to one of two NO_2 detection cells. The residence time between the heater and the detector was $\sim$ 0.4–0.5 s. The temperature ($\sim$ 60 °C) for the heated quartz was chosen by calculating the temperature that would maximize the amount of $CH_3O_2NO_2$ dissociated while minimizing the amount of HO_2NO_2 dissociated (Fig. 4). This also ensures that PAN and its analogs (e.g., PPN) did not dissociate in the $CH_3O_2NO_2$ channel. Dinitrogen pentoxide (N_2O_5) has similar thermodynamics to HO_2NO_2 at this temperature (Wooldridge et al., 2010); however, the typical N_2O_5 mixing

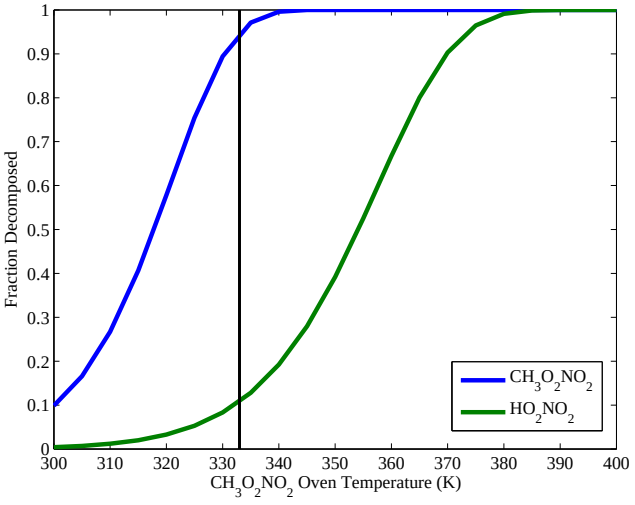

Figure 4. The calculated fractional decomposition of CH3O2NO2 (blue) and HO2NO2 (green) as a function of $CH_3O_2NO_2$ oven temperatures at a pressure of 230 hPa and a residence time of 0.08 s. The black line marks the target temperature ($\sim$ 60 °C) for optimal separation of $CH_3O_2NO_2$ and HO_2NO_2. Rates used to calculate the fraction decomposition are shown in Table 2.

ratio during the day is estimated to be small due to slow rates of production at night under the low-temperature conditions favorable to the presence of $CH_3O_2NO_2$.

The lower maximum temperatures of the $CH_3O_2NO_2$ and sum of peroxy nitrates (ΣPNs) heaters compared to the sum of alkyl and multifunctional nitrates (ΣANs) heaters (Fig. 5) allow for a simpler construction, as described in Wooldridge et al. (2010). Instead of bare nichrome wire, commercial woven fiberglass insulated heating cables are used, and thermo-

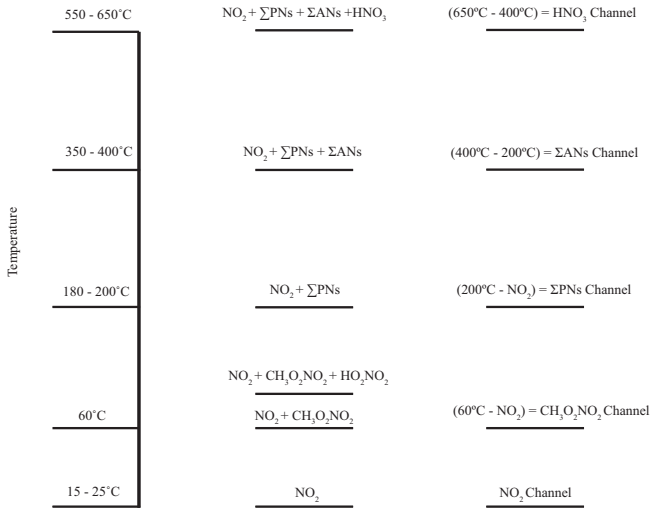

Figure 5. Schematic of the species measured in the TD-LIF channels and the temperature set points (temperatures the species dissociate) for those channels. ΣPNs $\equiv$ PAN + PPN + $CH_3O_2NO_2$ + HO_2NO_2 + ... and ΣANs $\equiv$ alkyl and multifunctional nitrates. The channel subtracted to calculate the measured species (e.g., $CH_3O_2NO_2$) is shown before the equals sign in the third column.

couples are fastened directly to the quartz tubes. The very small amount of heat required to bring the sample streams to 60 °C ($\sim$ 1 W for $CH_3O_2NO_2$, as calculated from the air heat capacity and mass flow rates) means that neither the maximum heater power (50 W across the 0.175 m heated length for $CH_3O_2NO_2$ dissociation) nor the quartz tube thermal resistance are limiting factors that would cause the thermocouple measurement to differ significantly from the internal gas temperature. Additionally, using the constant wall temperature approximation (e.g., Kliner et al., 1997; references therein), we calculate thermal equilibration lengths of 0.01–0.02 m for $CH_3O_2NO_2$, which are short compared to the overall heated lengths (0.175 m).

Mixing ratios of ambient $CH_3O_2NO_2$ are determined by subtracting the measurements from the NO_2 channel from the $CH_3O_2NO_2$ channel (60 °C, Fig. 5). Similarly, the mixing ratio of the ambient sum of peroxy nitrates (ΣPNs = PAN + PPN + $CH_3O_2NO_2$ + HO_2NO_2 + ...) is determined by subtracting the measurements from the NO_2 channel from the ΣPN channel, and the mixing ratio of ambient sum of alkyl and multifunctional nitrates (ΣANs) is determined by subtracting the measurements from the ΣPN channel from the ΣAN channel (Fig. 5). The HNO_3 channel depicted in Fig. 5 has been employed in other TD-LIF deployments, but was not part of the DC-3 and SEAC4RS configuration.

Table 1. Lengths for tubing in the corresponding sections for Fig. 3.

Campaign	Section A	Section B	Section C	NO_2 channel max residence time
ARCTAS	0.10 m	0.20 m	2.00 m	0.85 s
DC-3	0.10 m	0.08 m	1.50 m	0.50 s
SEAC4RS	1.00 m	0.12 m	0.30 m	0.23 s

2.2 NO_2 measurements free of non-acyl peroxy nitrate interference

Measuring NO_2 free of $CH_3O_2NO_2$ interference is desirable for understanding upper-tropospheric chemistry and essential to correctly derive the $CH_3O_2NO_2$ and ΣPN mixing ratios from the heated channels (Fig. 5). Measurements of NO_2 at ambient temperatures lower than 240 K, where non-acyl peroxy nitrates are more abundant due to longer thermal lifetimes (Fig. 1), are not free of interferences if the sample residence time in the aircraft is long (Browne et al., 2011). Figure 2 shows the calculated fraction of $CH_3O_2NO_2$ and HO_2NO_2 thermally dissociating in the NO_2 inlet prior to measuring NO_2 for different residence times and as a function of cabin temperature. At a cabin temperature of 300 K, approximately 90^{+5}_{-10}, 40^{+11}_{-6}, and 10^{+3}_{-2} % of $CH_3O_2NO_2$ and approximately 8$\pm$2, 2 %, and less than 1 % of HO_2NO_2 will thermally decompose at residence times of 2, 0.5, and 0.1 s, respectively. The uncertainties are based on the 2σ range reported for the decomposition rates of $CH_3O_2NO_2$ and HO_2NO_2. The partial thermal decomposition of $CH_3O_2NO_2$ and HO_2NO_2 can cause up to a 50 % increase in the measured NO_2 (XNO_2) vs. the ambient NO_2 (Fig. 2c).

2.3 Inlet configurations and effects on NO_2 and $CH_3O_2NO_2$ measurements

Figure 3 shows the schematic of the TD-LIF inlet. Table 1 lists the lengths and residence times of the different inlets used in three recent experiments: ARCTAS, DC-3, and SEAC4RS. The residence time is set by the measured length of tubing, the diameter of the tubing, and the flow speed of the sample pumps. Unless stated otherwise, the tubing has an internal diameter of $\sim$ 3.2 mm. Following the recommendations of Wooldridge et al. (2010) and Browne et al. (2011), we shortened the residence time for the NO_2 sample from 0.85 s during ARCTASto 0.5 s during DC-3, reducing the decomposition of $CH_3O_2NO_2$ in the NO_2 channel from $\sim$ 90 to $\sim$ 45 %.

To reduce the residence time further during SEAC4RS, a bypass pump was used to bring a large flow of ambient air through a 1 m, 15.9 mm i.d. tubing (Section A). We then reduced the length of Section C (Fig. 3, Table 1). The combined effects of these changes reduced the maximum residence time for NO_2 from 0.5 s (DC-3) to 0.23 s (SEAC4RS). This

Table 2. Reactions and rates used in calculating dissociations in instrument and photostationary steady-state calculations for $CH_3O_2NO_2$.

Reaction	Rate constant
$CH_3O_2NO_2 + M \rightleftharpoons CH_3O_2 + NO_2 + M$	Low-pressure limit $= 1.0 \times 10^{-30} \times (T/300)^{-4.8}$ High-pressure limit $= 7.2 \times 10^{-12} \times (T/300)^{-2.1}$ $K_{eq} = 9.5 \times 10^{-29} \times \exp(11234/T)$[a]
$HO_2NO_2 + M \rightleftharpoons HO_2 + NO_2 + M$	Low-pressure limit $= 2.0 \times 10^{-31} \times (T/300)^{-3.4}$ High-pressure limit $= 2.9 \times 10^{-12} \times (T/300)^{-1.1}$ $K_{eq} = 2.1 \times 10^{-27} \times \exp(10\,900/T)$[a]
$CH_3O_2NO_2 + h\nu \rightarrow CH_3O_2 + NO_2$	Assumed to be equal to measured HO_2NO_2 value
$CH_3O_2NO_2 + h\nu \rightarrow CH_3O + NO_3$	Assumed to be equal to measured HO_2NO_2 value
$CH_4 + OH \rightarrow CH_3O_2 + NO_2$	$2.45 \times 10^{-12} \times \exp(-1775/T)$[a]
$CH_3C(O)O_2 + NO \rightarrow CH_3O_2 + CO_2 + NO_2$	$8.1 \times 10^{-12} \times \exp(270/T)$[a]
$CH_3C(O)O_2 + CH_3C(O)O_2 + 2\,O_2 \rightarrow 2\,CH_3O_2 + 2\,CO_2 + O_2$	$2.9 \times 10^{-12} \times \exp(500/T)$[a]
$CH_3C(O)CH_3 + h\nu + O_2 \rightarrow CH_3C(O)O_2 + CH_3O_2$	Measured
$CH_3OOH + OH \xrightarrow{70\,\%} CH_3O_2 + H_2O$	$3.8 \times 10^{-12} \times \exp(200/T)$[a]
$CH_3C(O)OH + h\nu + O_2 \rightarrow CH_3O_2 + HCO$	Measured
$CH_3O_2 + NO \rightarrow CH_3O + NO_2$	$2.8 \times 10^{-12} \times \exp(300/T)$[a]
$CH_3O_2 + HO_2 \rightarrow$ Products	$3.8 \times 10^{-13} \times \exp(780/T)$[b]
$CH_3O_2 + CH_3C(O)O_2 \rightarrow$ Products	$2.0 \times 10^{-12} \times \exp(500/T)$[a]
$CH_3O_2 + CH_3O_2 \rightarrow$ Products	$9.5 \times 10^{-14} \times \exp(390/T)$[a]
$CH_3C(O)O_2NO_2 \rightleftharpoons CH_3C(O)O_2 + NO_2$	Low-pressure limit $= 9.7 \times 10^{-29} \times (T/300)^{-5.6}$ High-pressure limit $= 9.3 \times 10^{-12} \times (T/300)^{-1.5}$ $K_{eq} = 9.0 \times 10^{-29} \times \exp(14\,000/T)$[a]
$CH_3C(O)O_2NO_2 + h\nu \rightarrow CH_3C(O)O_2 + NO_2$	Measured
$CH_3C(O)OOH + OH \rightarrow CH_3C(O)O_2 + H_2O$	3.7×10^{-12} [c]
$CH_3C(O)H + OH + O_2 \rightarrow CH_3C(O)O_2 + H_2O$	$4.7 \times 10^{-12} \times \exp(345/T)$[b]
$CH_3C(O)O_2 + HO_2 \rightarrow$ Products	$5.2 \times 10^{-13} \times \exp(980/T)$[b]
$HO_2NO_2 + OH \rightarrow$ Products	$8.8 \times 10^{-19} \times T^2 \times \exp(1130/T)$[d]

[a] JPL 2011 (Sander et al., 2011); [b] Atkinson et al. (2006) (http://iupac.pole-ether.fr/htdocs/summary/vol2_summary.pdf); [c] Master Chemical Mechanism v3.2 (Saunders et al., 2003); [d] Jiménez et al. (2004).

reduced the factional thermal dissociation of $CH_3O_2NO_2$ in the NO_2 channel to $\sim 22\,\%$.

We obtain an NO_2 measurement by correcting for the partial thermal dissociation of $CH_3O_2NO_2$ in the XNO_2 channel (Eq. 1). The $CH_3O_2NO_2$ measurement is then determined by subtracting the corrected NO_2 and the fraction of thermally dissociated HO_2NO_2 in the $CH_3O_2NO_{2,CHANNEL}$ (Eq. 2) from the total signal in that channel.

$$NO_2 = XNO_2 - f_1 \times CH_3O_2NO_2 \quad (1)$$

$$CH_3O_2NO_2 = CH_3O_2NO_{2,CHANNEL} - NO_2 - f_2 \times HO_2NO_2 \quad (2)$$

To calculate the fraction of $CH_3O_2NO_2$ (f_1 in Eq. 1) that dissociates in the NO_2 sample line, we use the cabin temperature we measured near the TD-LIF NO_2 sample line along with the thermal rate constant (Table 2). To calculate the fraction of HO_2NO_2 (f_2 in Eq. 2) that has dissociated in the $CH_3O_2NO_2$ channel, we use the measured oven temperature ($\sim 60\,^\circ C$) along with the thermal rate constant (Table 2). With Eq. (1) and (2), we solve for the NO_2 and $CH_3O_2NO_2$ mixing ratios observed if there is an independent measurement or calculation of HO_2NO_2. During DC-3, the correction for the thermal dissociation of $CH_3O_2NO_2$ in XNO_2 ranged from 0 to 30 pptv (0 to 40 %) of the NO_2 mixing ratios at temperatures less than 240 K. During SEAC4RS, the correction ranged from 0 to 23 pptv (0 to 21 %). The correction for the thermal decomposition of HO_2NO_2 ranged from 0 to 20 pptv (0 to 11 %) for both campaigns.

2.4 Accuracy, uncertainty, and limit of detection for $CH_3O_2NO_2$

The accuracy of the $CH_3O_2NO_2$ measurements depends on the accuracy of our primary measurement of NO_2, the conversion efficiency in our inlet, and the interference of HO_2NO_2 in the $CH_3O_2NO_2$ channel. The uncertainty of the NO_2 calibration standard is $\sim 5\,\%$ (Sect. 2.1). Using the rate constant and 2σ uncertainty recommendation from JPL-2011 (Sander et al., 2011) at 60 °C, the thermal decomposition rate constant of $CH_3O_2NO_2$ is $36.0^{+19.0}_{-13.0}\,s^{-1}$, indicating between 85 and 99 % of $CH_3O_2NO_2$ is decomposed at this temperature and a residence time of 0.08 s. Including the uncertainty

estimated for the oven temperature (±5 °C), the amount of $CH_3O_2NO_2$ decomposed ranges from 70 to 100 %.

The transmission efficiency depends on recombination reactions and oxidation of NO. Day et al. (2002) and Wooldridge et al. (2010) showed these to be small effects (∼ 5–10 %) at NO mixing ratios less than 1 ppbv and pressures in the inlet region less than 400 hPa (ambient pressure). Assuming mixing ratios of 100 pptv for $CH_3O_2NO_2$ and HO_2NO_2, 200 pptv for NO_2, and 100–5000 pptv NO, we calculate a positive interference to $CH_3O_2NO_2$ measurements ranging from ∼ 8 to 26 % from the oxidation of NO to NO_2. The typical NO mixing ratios at the temperatures where $CH_3O_2NO_2$ is stable range from ∼ 50 to 400 pptv (25th–75th percentile), and for this range we calculate a positive interference of less than 10 %.

The similarity in the bond strength between HO_2NO_2 and $CH_3O_2NO_2$ (∼ 100 and ∼ 93 kJ mol^{-1}, respectively) prevents having a temperature set point that completely separates the two species (Fig. 4). For the oven temperature selected to decompose $CH_3O_2NO_2$ (60 °C) and the residence time in the oven (0.08 s), we calculate approximately 11^{+10}_{-6}% of HO_2NO_2 dissociates in the $CH_3O_2NO_2$ channel.

To summarize, the largest source of uncertainty in the $CH_3O_2NO_2$ measurement is the uncertainty of the thermal decomposition rate for $CH_3O_2NO_2$ (∼ 30 %). Other effects, including recombination reactions and the thermal decomposition of HO_2NO_2, are each typically less than 10 %. Combining these uncertainties, we estimate a total uncertainty of ±40 % for the $CH_3O_2NO_2$ measurements. We note that the sum of the NO_2 and $CH_3O_2NO_2$ measurement ($CH_3O_2NO_{2,CHANNEL}$) is more accurate (∼ 10 %) than the separate quantities.

The precision of the $CH_3O_2NO_2$ measurements depends on the shot noise of the photon-counting rate, the precision of the NO_2 measurement, the concentration of NO_2, and the concentration of $CH_3O_2NO_2$. Using the median NO_2 measured between 10 and 11 km (∼ 200 pptv of NO_2), and using the lower end of the sensitivity observed during DC-3 (0.100 cts pptv^{-1}), the detection limit for $CH_3O_2NO_2$ is 15 pptv at 60 s^{-1} for $S/N = 2$. The median limit of detection ($S/N = 2$ and 60 s averaged data) for the DC-3 campaign is shown vs. altitude in Fig. 10b (red line).

3 Ambient measurements of $CH_3O_2NO_2$

$CH_3O_2NO_2$ measurements obtained during the DC-3 (2012) and SEAC4RS (2013) campaigns are located in NASA's publicly accessible archives: http://www-air.larc.nasa.gov/cgi-bin/ArcView/dc3-seac4rs and https://www-air.larc.nasa.gov/cgi-bin/ArcView/seac4rs.

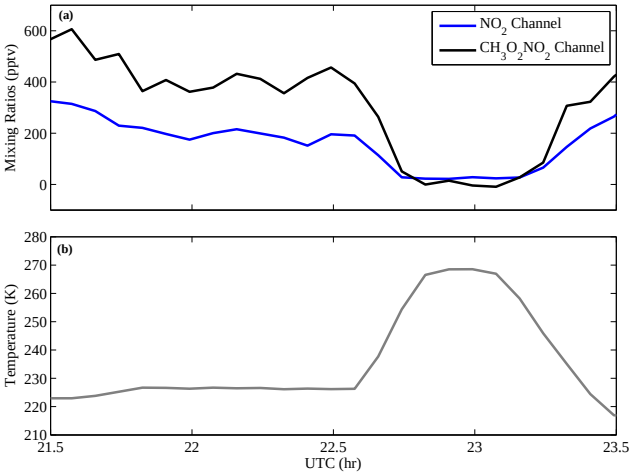

Figure 6. Five-minute-averaged time series of **(a)** NO_2 (blue) and $CH_3O_2NO_2$ (black) channel and **(b)** temperature from a flight on 17 June 2012 during DC-3. The local time was approximately midafternoon during this time segment.

3.1 Characterization of the measurements of ambient $CH_3O_2NO_2$

We utilize the measurements collected during DC-3 to validate the temperature selected to fully decompose $CH_3O_2NO_2$ with minimal interference from thermally decomposed HO_2NO_2. First, we ensure that the $CH_3O_2NO_2$ channel behaves as expected: at high ambient temperatures (low altitudes) the $CH_3O_2NO_2$ channel should only be detecting ambient NO_2 (Fig. 1), but at low ambient temperatures (high altitudes), the $CH_3O_2NO_2$ channel should be detecting NO_2 from both ambient NO_2 and thermally decomposed $CH_3O_2NO_2$. This behavior is observed, as shown in an example flight from DC-3 (Fig. 6).

We utilize observations of $CH_3O_2NO_2$ near the limit of detection (Fig. 7 between ∼ 21:30 and 22:00 UTC) to calculate an upper limit for the thermal dissociation of HO_2NO_2 in the $CH_3O_2NO_2$ channel. The median observed HO_2NO_2 is 94^{+11}_{-35} pptv (plus 75th quartile and minus 25th quartile). In the $CH_3O_2NO_2$ channel, we observed 24^{+10}_{-6} pptv (median and interquartile). Assuming zero for the $CH_3O_2NO_2$ mixing ratio, this gives an upper limit to the HO_2NO_2 present in the $CH_3O_2NO_2$ of ∼ 25 % of the measured HO_2NO_2. Calculations (Sect. 2.4) suggest the most likely amount of HO_2NO_2 thermally dissociated is ∼ 11 %, with an upper limit based on propagating uncertainties in rate constants of 25 to 30 %. The observed values are consistent with this upper limit. We conclude that some (∼ 6 pptv calculated assuming photostationary steady state) $CH_3O_2NO_2$ should be present. If we assume this $CH_3O_2NO_2$ is correct, the HO_2NO_2 fraction dissociated is ∼ 20 %.

Another way to determine if the temperature selected fully decomposes $CH_3O_2NO_2$ with minimal HO_2NO_2

Table 3. Measurements used in this analysis and calculations of the lifetimes in Fig. 1.

Species	Method	Reference
NO_2, $CH_3O_2NO_2$, ΣPNs	Thermal-dissociation laser-induced fluorescence	Thornton et al. (2000), Day et al. (2002)
HO_2NO_2, PAN, PPN	Chemical ionization mass spectrometry	Slusher et al. (2004), Kim et al. (2007)
OH, HO_2	Laser-induced fluorescence	Faloona et al. (2004)
UV photolytic frequencies	Spectral radiometry	Shetter and Müller (1999)

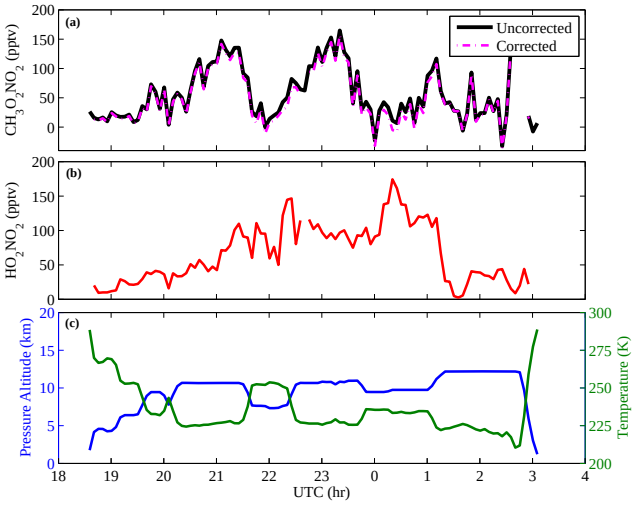

Figure 7. Five-minute-averaged time series of **(a)** uncorrected (black) and corrected (magenta) $CH_3O_2NO_2$ for HO_2NO_2 thermal decomposition, **(b)** HO_2NO_2, and **(c)** pressure altitude (blue) and temperature (green) from a flight on 30 May 2012 during DC-3. Local sunset is approximately 00:00 UTC.

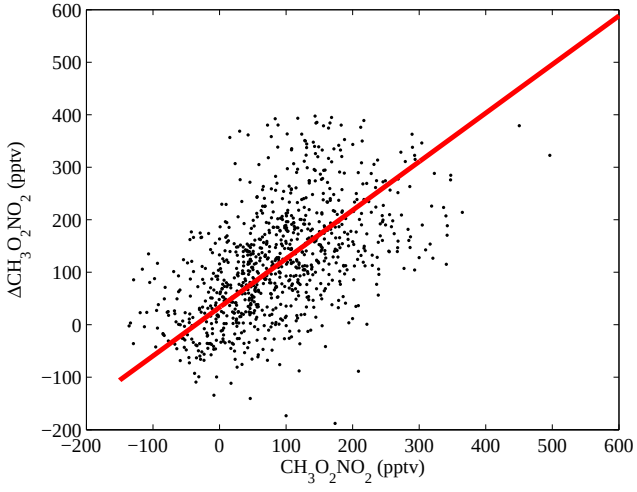

Figure 8. $CH_3O_2NO_2$ inferred ($\Delta CH_3O_2NO_2$) as the difference of the total peroxy nitrates minus PAN, PPN, and HO_2NO_2 compared to $CH_3O_2NO_2$ observed by TD-LIF at temperatures between 220 and 230 K (Table 3). The red line is a weighted fit to the data: slope of 0.93 (±0.07) and intercept of −33.0 (±5.9) pptv. The uncertainties used in the calculations are ±40 % + 20 pptv for $CH_3O_2NO_2$, ±15 % + 20 pptv for SPNs, ±15 % + 2 pptv for PAN, ±20 % + 1 pptv for PPN, and ±30 % + 1 pptv for HO_2NO_2. The R^2 of the fit is 0.3.

decomposition is to compare inferred $CH_3O_2NO_2$ ($CH_3O_2NO_{2(inferred)} \equiv$ ΣPNs–(HO_2NO_2 + PAN + PPN)) to measured $CH_3O_2NO_2$ during the DC-3 campaign (Fig. 8). PAN, PPN, and HO_2NO_2 were measured by chemical ionization-mass spectrometry (Table 3; Slusher et al., 2004; Kim et al., 2007). The observations used are one minute merged data from temperatures between 220 and 230 K, where the signal of the $CH_3O_2NO_2$ measurements is well above the noise (Fig. 10b). Using weighted (by accounting for differing uncertainties in the individual points) bivariate least-squares fit (Cantrell, 2008), we calculated a slope of 0.93 (±0.07) after removing a few (378 of 1296 data points) $CH_3O_2NO_{2(inferred)}$ points more than ±3 standard deviations from the median. While the $CH_3O_2NO_{2(inferred)}$ is not completely independent from $CH_3O_2NO_2$, as both $CH_3O_2NO_2$ and ΣPNs are measured by the same technique, the fact that the slope is nearly 1 indicates that the temperature selected for the $CH_3O_2NO_2$ channel is high enough to thermally decompose all $CH_3O_2NO_2$, supporting the conclusion that the thermally decomposed HO_2NO_2 is less than the upper limit (25–30 %) calculated above. Also, the slope implies that the direct $CH_3O_2NO_2$ measurement is accurate to at least the ±40 % estimated above.

3.2 Examples of measurements of $CH_3O_2NO_2$

A time series of $CH_3O_2NO_2$ during the flight of 30 May 2012 is shown in Fig. 7. The flight of 30 May 2012 sampled the aging of deep convective outflow affected by lightning NO_x. The time series shows the variability in the $CH_3O_2NO_2$ measurements that corresponds to the temperature of the ambient air, location of the DC-8, and chemical aging of the convective outflow. Prior to approximately 01:00 UTC, the DC-8 was sampling different altitudes to characterize the aging of convective outflow. At higher altitudes (ambient temperatures less than 230 K), the mean $CH_3O_2NO_2$ was ∼ 100 pptv and ranged from ∼ 26 to 165 pptv. At lower altitudes (ambient temperatures between 230 and 260 K), the mean $CH_3O_2NO_2$ was ∼ 35 pptv and ranged from 0 to 95 pptv.

At these lower altitudes, where the HO_2NO_2 measurements are higher (range ∼ 20–170 pptv) than the $CH_3O_2NO_2$ mixing ratios, the structure in the $CH_3O_2NO_2$ measurements is not simply a mirror of the HO_2NO_2 measurements. If there were a large interference from the thermal decomposition of HO_2NO_2 in the $CH_3O_2NO_2$ channel, we would expect to see a similar structure in the two measurements. For example, between 00:00 and 01:00 UTC, the HO_2NO_2 mixing ratio peaks at ∼ 170 pptv, whereas at the same time the $CH_3O_2NO_2$ decreases to ∼ 10 pptv. The largest corrections for the thermal decomposition of HO_2NO_2 in the $CH_3O_2NO_2$ channel occur at lower altitudes (Fig. 6a), where $CH_3O_2NO_2$ lifetime is short (Fig. 1). This gives us further confidence that the thermal decomposition of HO_2NO_2 is a small interference in the measurement of $CH_3O_2NO_2$.

At 01:00 UTC, the DC-8 started sampling stratospheric air. The $CH_3O_2NO_2$ mixing ratios dropped to ∼ 30 pptv (range 0–140 pptv). This is lower than the values observed in the upper troposphere at ambient temperatures less than 230 K. Even though the temperatures in the lower stratosphere are low enough for the $CH_3O_2NO_2$ lifetime to be greater than 10 h, the observations of $CH_3O_2NO_2$ indicate that the lower stratosphere has lower mixing ratios of the precursors of CH_3O_2 needed to form $CH_3O_2NO_2$. These include the peroxy acyl radical from acetaldehyde, which reacts with NO to produce CH_3O_2 (e.g., Tyndall et al., 2001), and CH_3COCH_3, which can photolyze to produce CH_3O_2 (e.g., Folkins and Chatfield, 2000; Jaeglé et al, 2001; Neumaier et al., 2014).

An example of $CH_3O_2NO_2$ behaving as an important NO_x reservoir downwind of deep convection is shown in Fig. 9. We observed the production of $CH_3O_2NO_2$ in the aging outflow of deep convection during the flight of 21 June 2012 (Fig. 9). The DC-8 sampled at a constant ambient temperature (∼ 225 K) and entered the outflow between 12:00 and 13:00 UTC (0–1 h chemically aged), where the $CH_3O_2NO_2$ mixing ratio was observed to be ∼ 0 pptv. The aircraft sampled the outflow until ∼ 16:30 UTC (4.5 h chemically aged), where the $CH_3O_2NO_2$ mixing ratio was observed to be ∼ 150 pptv. The apparent $CH_3O_2NO_2$ production rate was ∼ 60 pptv h^{-1} – an indication of the importance of this chemistry to understanding upper-tropospheric chemistry.

We compare the median $CH_3O_2NO_2$ profiles during DC-3 (black), SEAC4RS (dark grey) and ARCTAS-A (blue, as calculated by Browne et al., 2011) in Fig. 10b. At altitudes above 7 km, higher mixing ratios of $CH_3O_2NO_2$ were observed during both DC-3 and SEAC4RS compared to ARCTAS-A due to the influence of deep convection, lightning NO_x, and biomass burning. Also, DC-3 and SEAC4RS occurred later in the year (May–June 2012 for DC-3 and August–September 2013 for SEAC4RS) than ARCTAS-A (April 2008); thus, photochemistry is more active, producing more $CH_3O_2NO_2$. This is consistent with calculations described by Browne et al. (2011), who found modeled $CH_3O_2NO_2$ mixing ratios to be higher in the summer than spring. Finally, the observed $CH_3O_2NO_2$ during SEAC4RS

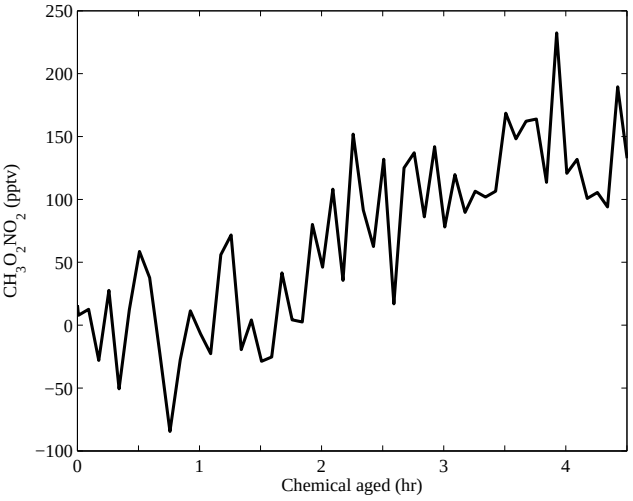

Figure 9. Five-minute-averaged time series of the chemical evolution of $CH_3O_2NO_2$ downwind from convection from a flight on 21 June 2012 during DC-3. The *x* axis shows the age of the air parcel that the DC-8 started sampling at approximately 12:00 UTC (0 h), which was the local sunrise.

at lower altitudes is higher due to the impact of agricultural and biomass burning. Higher NO_2 mixing ratios from biomass burning shift the equilibrium towards $CH_3O_2NO_2$, similar to the higher NO_2 concentrations shifting the equilibrium towards HO_2NO_2 production near an urban area (Spencer et al., 2009). Higher $CH_3O_2NO_2$ mixing ratios due to biomass burning are also consistent with the GEOS-Chem results from Browne et al. (2011).

During DC-3, $CH_3O_2NO_2$ measurements dropped to below the limit of detection at high altitudes (> 11.5 km) when the aircraft was sampling the stratosphere. The stratosphere is higher during SEAC4RS since the campaign occurs later in the season; thus, higher mixing ratios of $CH_3O_2NO_2$ are observed.

Finally, we compare the calculated instantaneous steady-state mixing ratios of $CH_3O_2NO_2$ to measured $CH_3O_2NO_2$ during DC-3 (Fig. 11). We limit the comparison to observations for which the calculated lifetime of $CH_3O_2NO_2$ is less than 10 h, the tropospheric composition has not been recently perturbed by fresh NO_x emissions ($NO_x / NO_y < 0.4$) or stratospheric intrusions ($O_3 / CO < 1.25$), and to solar zenith angles less than 85° – all conditions that make it more likely that steady state is achieved in the atmosphere. We used only observations at temperatures less than 250 K where $CH_3O_2NO_2$ is thermally stable. The comparison is also restricted to observations where the $CH_3O_2NO_2$ signal is greater than the noise (Fig. 10b). Observations with $CH_3O_2NO_2 / NO_2$ greater than 1 are excluded as they are also indicative of an air mass that is not in steady state. The reactions used in the model are listed in Table 2. Within the variability and uncertainty of the measured and calculated $CH_3O_2NO_2$ mixing ratios, the calculated values are nearly

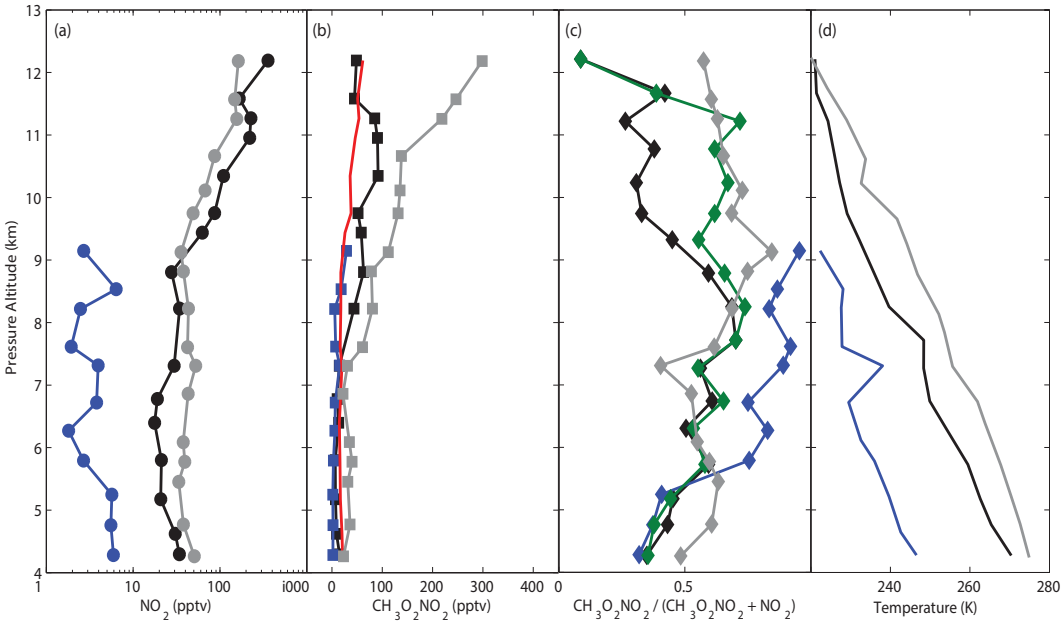

Figure 10. The median profile of **(a)** NO_2, **(b)** $CH_3O_2NO_2$, **(c)** $CH_3O_2NO_2/(NO_2+CH_3O_2NO_2)$, and **(d)** temperature for ARCTAS-A (blue), DC-3 (black), and SEAC4RS (dark grey). The red line in **(b)** is the median limit of detection for $S/N = 2$, 60 s for DC-3. The green line in **(c)** is the median $CH_3O_2NO_2/(NO_2+CH_3O_2NO_2)$ in background air where NO_x/NO_y is less than 0.2 during DC-3.

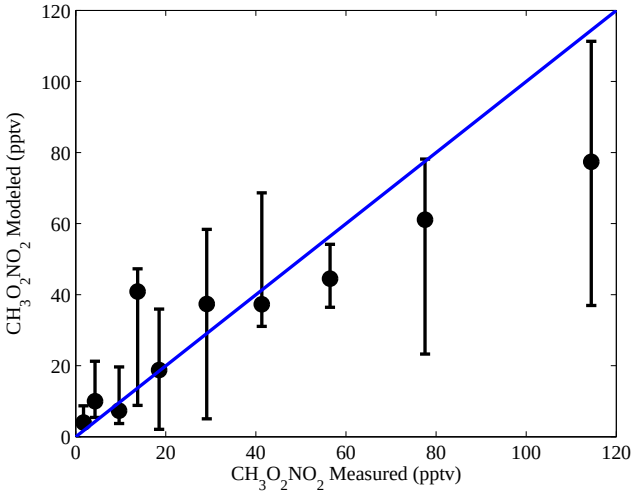

Figure 11. Binned modeled vs. measured $CH_3O_2NO_2$. The bars identify the interquartile of the modeled $CH_3O_2NO_2$. The blue line has a slope of 1 for reference.

the same as the measured values (median values falling near the one-to-one line). This agreement indicates that, for air parcels in photostationary state, the chemistry and kinetics are understood to within ∼ 50 %. This also provides us with further confidence in the laboratory measurements of $CH_3O_2NO_2$ rate constants that we use as a guide to instrument design and evaluation.

4 Discussion

We observe that $CH_3O_2NO_2$ composed 7 % and HO_2NO_2 composed 5 % of the median NO_y budget between 220 and 230 K during DC-3, where NO_y is defined as the sum of NO_x, ΣPNs, ΣANs, and HNO_3. This is significant since many transport models neglect $CH_3O_2NO_2$ chemistry. During DC-3, these weakly bound species comprised a larger portion of the median NO_y budget than HNO_3 (4 %), which is a terminal sink for NO_x. In prior analysis of tropospheric air cooler than 240 K, Murphy et al. (2004) calculated the sum of HO_2NO_2 and $CH_3O_2NO_2$ as the difference between ΣPNs measured by TD-LIF, and PAN and PPN measured using gas chromatography with electron capture detection (similar to $CH_3O_2NO_{2(\text{inferred})}$ above). Murphy et al. (2004) reported these two species were a large fraction of the NO_y budget at temperatures cooler than 240 K (17–22 %), impacting NO_x and radical chemistry. That the percent composition for the non-acyl peroxy nitrates during DC-3 were lower than reported by Murphy et al. (2004) is not surprising because the sampling during DC-3 was biased toward fresh convective outflow impacted by lightning NO_x, meaning NO_x composed 39 % of the NO_y budget vs. the 5 % for the air observed by Murphy et al. (2004). For background air ($NO_x/NO_y < 0.2$) observed during DC-3, $CH_3O_2NO_2$ composed a larger portion of the median NO_y budget (12 %), and the median non-acyl peroxy nitrate portion of the NO_y budget ($CH_3O_2NO_2+HO_2NO_2$ (5 %)) had a sum that is similar to the observations by Murphy et al. (2004) of 17 %.

The lower NO_x mixing ratios characteristic of the air observed by Murphy et al. (2004) were also characteristic of the air observed by Browne et al. (2011) during ARCTAS-A, as both were springtime measurements in the Arctic. The comparison of ARCTAS-A, DC-3, and SEAC4RS is shown in Fig. 10. The lower NO_2 mixing ratios observed during ARCTAS-A meant the air masses were more dominated by $CH_3O_2NO_2$ than by NO_2 ($CH_3O_2NO_2 / (NO_2 + CH_3O_2NO_2)$ ratios closer to 1.0, Fig. 10c). The dominance of $CH_3O_2NO_2$ means that it is an important source of NO_2, and that is an important interference for ambient NO_2 measurements. In DC-3, the influence of lightning NO_x emissions made the median air masses for the entire campaign more dominated by NO_2 (ratios less than 0.5). The median $CH_3O_2NO_2 / (NO_2 + CH_3O_2NO_2)$ ratios are slightly smaller than the ratios calculated in the GEOS-Chem model from Browne et al. (2011) for air influenced by deep convection and lightning. In background air sampled by the DC-8 during DC-3, the median $CH_3O_2NO_2 / (NO_2 + CH_3O_2NO_2)$ ratio was in the range 0.3 to 0.7 (Fig. 10c, green). We observed similar median ratios during SEAC4RS (Fig. 10c, dark grey). These values are closer to the values calculated during ARCTAS (Fig. 10c, blue; Browne et al., 2011). This indicates that, with aging, the ratio shifts toward air more dominated by $CH_3O_2NO_2$, impacting the ozone chemistry of the upper troposphere, as previously described by Browne et al. (2011).

5 Conclusions

We report the first measurements of atmospheric $CH_3O_2NO_2$ and report recommendations for instrument design to sample NO_2 free of interferences from thermal decomposition of non-acyl peroxy nitrates. We conclude that, for an instruments where the sample lines and/or detection region is at a temperature of 300 K, total residence times of less than 0.1 s are required to keep the interference to NO_2 below 10 % of $CH_3O_2NO_2$ and below 1 % of HO_2NO_2. We describe a procedure for evaluating the interference of $CH_3O_2NO_2$ in NO_2 using measurements of $CH_3O_2NO_2$. Our measurements show that for temperatures less than 230 K the median $CH_3O_2NO_2$ is a larger fraction of NO_y than HNO_3, experimental evidence for the important role of $CH_3O_2NO_2$ in the upper troposphere. Our measurements also provide supporting evidence for the conclusion of Browne et al. (2011), who predicted larger $CH_3O_2NO_2$ mixing ratios in summer than in spring using GEOS-CHEM.

Acknowledgements. This research was funded by NASA grant NNX12AB79G and based upon work supported by the National Science Foundation Graduate Research Fellowship under grant no. DGE 1106400 to B. A. Nault. S. E. Pusede acknowledges support from the NASA Postdoctoral Program. We thank William H. Brune for use of the OH and HO_2 measurements, L. Gregory Huey for the use of Georgia Institute of Technology CIMS data, Paul O. Wennberg for the use of HNO_3 data, and Thomas B. Ryerson for the use of NO data. We also thank the ground and flight crews of the DC-8 and DC-3 and SEAC4RS science team.

Edited by: H. Harder

References

Atkinson, R., Baulch, D. L., Cox, R. A., Crowley, J. N., Hampson, R. F., Hynes, R. G., Jenkin, M. E., Rossi, M. J., Troe, J., and IUPAC Subcommittee: Evaluated kinetic and photochemical data for atmospheric chemistry: Volume II – gas phase reactions of organic species, Atmos. Chem. Phys., 6, 3625–4055, doi:10.5194/acp-6-3625-2006, 2006.

Browne, E. C., Perring, A. E., Wooldridge, P. J., Apel, E., Hall, S. R., Huey, L. G., Mao, J., Spencer, K. M., Clair, J. M. St., Weinheimer, A. J., Wisthaler, A., and Cohen, R. C.: Global and regional effects of the photochemistry of $CH_3O_2NO_2$: evidence from ARCTAS, Atmos. Chem. Phys., 11, 4209–4219, doi:10.5194/acp-11-4209-2011, 2011.

Cantrell, C. A.: Technical Note: Review of methods for linear least-squares fitting of data and application to atmospheric chemistry problems, Atmos. Chem. Phys., 8, 5477–5487, doi:10.5194/acp-8-5477-2008, 2008.

Cleary, P. A., Wooldridge, P. J., and Cohen, R. C.: Laser-induced fluorescence detection of atmospheric NO_2 with a commercial diode laser and a supersonic expansion, Appl. Optics, 41, 6950–6956, 2002.

Day, D. A., Wooldridge, P. J., Dillon, M. B., Thornton, J. A., and Cohen, R. C.: A thermal dissociation laser-induced fluorescence instrument for in situe detection of NO_2, peroxy nitrates, alkyl nitrates, and HNO_3, J. Geophys. Res., 107, 4046, doi:10.1029/2001JD000779, 2002.

Diskin, G. S., Podolske, J. R., Sachse, G. W., and Slate, T. A.: Open-Path Airborne Tunable Diode Laser Hygrometer, in: Diode Lasers and Applications in Atmospheric Sensing, edited by: Fried, A., SPIE Proceedings, 4817, 196–204, 2002.

Faloona, I. C., Tan, D., Lesher, R. L., Hazen, N. L., Frame, C. L., Simpas, J. B., Harder, H., Martinez, M., Di Carlo, P., Ren, X., and Brune, W. H.: A laser-induced fluorescence instrument for detecting tropospheric OH and HO_2: Characteristics and calibration, J. Atmos. Chem., 47, 139–167, 2004.

Folkins, I. and Chatfield, R.: Impact of acetone on ozone production and OH in the upper troposphere at high NO_x, J. Geophys. Res., 105, 11585–11599, doi:10.1029/2000JD900067, 2000.

Jaeglé, L., Jacob, D. J., Brune, W. H., and Wennberg, P. O.: Chemistry of HO_x radicals in the upper troposphere, Atmos. Environ., 35, 469–489, doi:10.1016/S1352-2310(00)00376-9, 2001.

Jiménez, E., Gierczak, T., Stark, H., Burkholder, J. B., and Ravishankara, A. R.: Reaction of OH with HO_2NO_2 (Peroxynitric Acid): Rate Coefficients between 218 and 335 K and Product Yields at 298 K, J. Phys. Chem. A., 108, 1139–1149, doi:10.1021/jp0363489, 2004.

Kliner, D. A. V., Daube, B. C., Burley, J. D., and Wofsy, S. C.: Laboratory investigation of the catalytic reduction technique for measurement of atmospheric NO_y, J. Geophys. Res., 102, 10759–10776, doi:10.1029/96JD03816, 1997.

Kim, S., Huey, L. G., Stickel, R. E., Tanner, D. J., Crawford, J. H., Olson, J. R., Chen, G., Brune, W. H., Ren, X., Lesher, R., Wooldridge, P. J., Bertram, T. H., Perring, A., Cohen, R. C., Lefer, B. L., Shetter, R. E., Avery, M., Diskin, G., and Sokolik, I.: Measurement of HO_2NO_2 in the free troposphere during the Intercontinental Chemical Transport Experiment – North America 2004, J. Geophys. Res., 112, D12S01, doi:10.1029/2006Jd007676, 2007.

Murphy, J. G., Thornton, J. A., Wooldridge, P. J., Day, D. A., Rosen, R. S., Cantrell, C., Shetter, R. E., Lefer, B., and Cohen, R. C.: Measurements of the sum of HO_2NO_2 and $CH_3O_2NO_2$ in the remote troposphere, Atmos. Chem. Phys., 4, 377–384, doi:10.5194/acp-4-377-2004, 2004.

Neumaier, M., Ruhnke, R., Kirner, O., Ziereis, H., Stratmann, G., Brenninkmeijer, C. A. M., and Zahn, A: Impact of acetone (photo)oxidation on HO_x production in the UT/LMS based on CARIBIC passenger aircraft observations and EMAC simulations, Geosphy. Lett., 41, 3289–3297, doi:10.1002/2014GL059480, 2014.

Sander, S. P., Abbatt, J. Barker, J. R., Burkholder, J. B., Friedl, R. R., Golden, D. M., Huie, R. E., Kolb, C. E., Kurylo, M. J., Moortgat, G. K., Orkin, V. L., and Wine, P. H.: Chemical Kinetics and Photochemical Data for Use in Atmospheric Studies, Evaluation Number 17, JPL Publication 10-6, Jet Propulsion Laboratory, Pasadena, 2011.

Saunders, S. M., Jenkin, M. E., Derwent, R. G., and Pilling, M. J.: Protocol for the development of the Master Chemical Mechanism, MCM v3 (Part A): tropospheric degradation of non-aromatic volatile organic compounds, Atmos. Chem. Phys., 3, 161–180, doi:10.5194/acp-3-161-2003, 2003.

Shetter, R. E. and Müller, M.: Photolysis frequency measurements using actinic flux spectroradiometry during the PEM-Tropics Mission: Instrument description and some results, J. Geophys. Res., 104, 5647–5661, 1999.

Slusher, D., Huey, L. G., Tanner, D. J., Flocke, F. M., and Roberts, J. M.: A thermal dissociation chemical ionization mass spectrometry (TD-CIMS) technique for the simultaneous measurements of peroxacyl nitrates and dinitrogen pentoxide, J. Geophys. Res., 109, D19315, doi:10.1029/2004JD004670, 2004.

Spencer, K. M., McCabe, D. C., Crounse, J. D., Olson, J. R., Crawford, J. H., Weinheimer, A. J., Knapp, D. J., Montzka, D. D., Cantrell, C. A., Hornbrook, R. S., Mauldin III, R. L., and Wennberg, P. O.: Inferring ozone production in an urban atmosphere using measurements of peroxynitric acid, Atmos. Chem. Phys., 9, 3697–3707, doi:10.5194/acp-9-3697-2009, 2009.

Thornton, J. A., Wooldridge, P. J., and Cohen, R. C.: Atmospheric NO_2: In situ laser-induced fluorescence detection at parts per trillion mixing ratios, Anal. Chem., 72, 528–539, 2000.

Tyndall, G. S., Cox, R. A., Granier, C., Lesclaux, R., Moortgat, G. K., Pilling, M. J., Ravishankara, A. R., and Wallington, T. J.: Atmospheric chemistry of small organic peroxy radicals, J. Geophys. Res., 106, 12157–12182, 2001.

Wooldridge, P. J., Perring, A. E., Bertram, T. H., Flocke, F. M., Roberts, J. M., Singh, H. B., Huey, L. G., Thornton, J. A., Wolfe, G. M., Murphy, J. G., Fry, J. L., Rollins, A. W., LaFranchi, B. W., and Cohen, R. C.: Total Peroxy Nitrates (ΣPNs) in the atmosphere: the Thermal Dissociation-Laser Induced Fluorescence (TD-LIF) technique and comparisons to speciated PAN measurements, Atmos. Meas. Tech., 3, 593–607, doi:10.5194/amt-3-593-2010, 2010.